



PII: S0020-7403(96)00071-9

EFFECTS OF WATER-MIXTURE FILM ON IMPACT CONTACT IN ABRASIVE WATERJET MACHINING

Z. YONG and R. KOVACEVIC

Center for Robotics and Manufacturing Systems University of Kentucky, KY 40506-0108, U.S.A.

(Received 6 July 1995; in revised form 20 June 1996)

Abstract—The effects of a water-mixture film adhering to solid materials on the impact contact are examined by employing exact solutions for an inhomogeneous contact problem and the Hertz impact theory. The elastic modulus of the water on a surface is assumed to be zero and the modulus of the water-mixture between a water surface and a target material varies from zero to the modulus of the target material. Non-elastic deformation is considered based on an energy balance. A new expression of closed form for impact force is obtained. The film effect on the impact force is very significant for low impact energy and becomes stable and less influential once impact energy increases to a certain value. Experimental results for quasi-static force are in agreement with the theoretical analysis in which two unknown parameters are ascertained by experiments. The minimum effective velocity of garnet abrasives achieved in this work for waterjet machining is consistent with previous results. Copyright © 1997 Elsevier Science Ltd.

Keywords: impact contact, film, machining.

NOTATION

E_1, E_2	elastic moduli of two contact bodies with no film
E_{z1}, E_{z2}	variable moduli of two inhomogeneous bodies
E_I, E_{II}	elastic constants relevant to E_1, E_2
g	gravity acceleration
h	film thickness between two contact bodies
h_i	water-mixture film thickness of a contact body ($i = 1, 2$)
H	height of a freely-falling ball
k_0	stiffness of an elastic contact system
M	mass of a moving body
M_p	mass of an abrasive
P_r	static contact force
P_m	maximum impact force
P_{mF}	maximum impact force with film
r_p	ratio of impact force for dry contact to impact force for film contact
V_0	velocity of a moving body
V_p	minimum effective velocity of an abrasive in waterjet

Greek letters

α	material exponent relevant to E_{zi} ($i = 1, 2$)
δ_0	static elastic displacement between two contact bodies
δ_m	maximum dynamic displacement between two contact bodies
ν_1, ν_2	Poisson's ratios of two contact bodies

1. INTRODUCTION

Impact contact problems caused by the presence of a water-mixture film is an inherent characteristic of the abrasive waterjet (AWJ) machining process. During the machining operation, abrasives carried by a water stream strike a target material and hence surfaces of both the abrasives and target are coated by a water film. Through particle fragmentation and the cutting action, many tiny powder particles are produced forming a water-mixture film which remains above or on the target surface before it is transported away by water flow. The mixture consists of two types of particles. One is chips of target material and the other is powder fragments of worn or broken abrasives.

For the case of dry contact, mechanisms of abrasive fragmentation have been both theoretically and experimentally examined in recent work [1, 2] regarding the interference between particles and

targets and the collision between particles in flow [3]. Additionally, microscopic observations of powder samples removed from cast iron specimens by AWJ show that the scale of numerous powder particles of cast iron is much smaller than garnet abrasives with the size of mesh 80 [4]. This evidence suggests that before impinging a target, an abrasive could first encounter a water-mixture film which may consume considerable kinetic energy of the abrasive so that the amplitude of impact force caused by the abrasive may be reduced.

More experimental results to support this analysis can be found in the work [5] which uses the acoustic emission technique. According to their results, acoustic emission signals for the full penetration cutting of an aluminum specimen are much larger than signals for the partial penetration cutting. Furthermore, for the partial cutting, the signals received at the entrance and exit stages are significantly greater than the signals received during the middle cutting stage. An analysis of on-site conditions shows that the only cause for the large difference of signals is the variation of water flow conditions with the cutting depth and distance from the target surface. In other words, different flow conditions around the cut surface influence the thickness of the water-mixture film and other properties of the film. In particular, when AWJ is used for drilling, the water-mixture film could have a severe influence on the amplitude of impact force. Evidently, obtaining an accurate estimation of impact force is an important initial step in quantitative investigations of topics relevant to AWJ machining, such as fragmentation analysis of materials [6, 7]. In general, a better understanding of the underlying mechanisms of the film effect will be helpful for accounting for and controlling the machining process of AWJ.

Regardless of the powder mixture, the effects of water film adhering to abrasives on the consumption of impact energy is not a new topic. For instance, considering radial fluid velocity in the squeeze film, research [8] has revealed that the one-phase squeeze film separating the advanced particle from the surface consumes considerable kinetic energy from the particle when the Reynolds number is relatively low. It will be seen from this investigation that a similar effect still holds for the mixture film although the approach developed here differs greatly from the one in [8].

In comparison with dry impact contact or wet contact with one-phase film, which has been extensively discussed by many researchers [2, 8–13], very little research for impact contact with a water-mixture film has been done despite its practical benefits. From the contact mechanics point of view, one of the main reasons for the current situation is possibly the lack of an effective theoretical approach. Strictly speaking, this is a three-phase interaction problem. The solid phase consists of abrasives and a target material, the liquid phase is water and the powder particles removed from the target and abrasives next to the surface of the target are categorized into the third phase referred to as the mixture phase. Obviously, any attempt to rigorously quantify the impact process would face many formidable challenges.

In the present work, the impact contact problem of three phases is simplified to a central impact contact problem of two inhomogeneously-layered solid bodies by employing exact solutions for an inhomogeneous elastic contact problem [14] and the Hertz impact contact theory [15]. The non-elastic portion of energy is calculated through a general equation of energy balance. Theoretical results for impact force are consistent with experimental data.

2. THEORETICAL ANALYSIS

Before discussing the theoretical derivations, some concepts about the physical background of this approach are briefly introduced as follows.

As shown in Fig. 1, elastic moduli of two inhomogeneous contact bodies are $E_{z1} = E_1|z|^\alpha$ and $E_{z2} = E_2|z|^\alpha$ ($0 \leq \alpha < 1$), respectively. On the surface of $z = 0$ both E_{z1} and E_{z2} are zero which corresponds to the elastic property of water. The relation $E_z/E = |2z/h|^\alpha$ is plotted in Fig. 2 where $h/2$ denotes the thickness of a water-mixture film on a body. Clearly, the larger α is, the softer the material could become. Note that if $0 < \alpha \leq 0.1$, the elastic property of a contact body is rapidly changed from zero, the liquid phase, to a certain modulus E of $z = h/2$, the solid phase. The middle part of $0 < z < h/2$, which is softer than solid but harder than water, represents the mixture phase made of powder mixture and water. Meanwhile, there is no evident increase of E_z after $z > h/2$. Therefore, it is suitable to apply general results for the inhomogeneous contact problem [14] to simulate the effects of a water-mixture film. In this circumstance, if the elastic moduli of the two solids with no film are denoted by E_1 and E_2 , respectively, E_{z1} and E_{z2} are

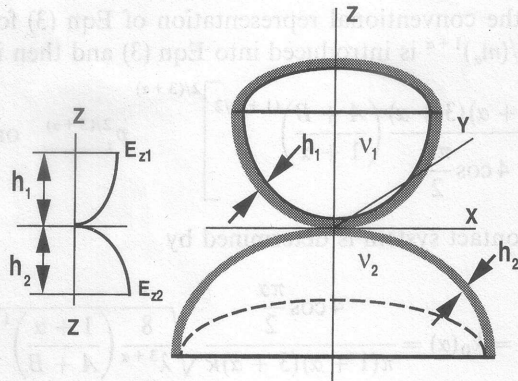


Fig. 1. Two elastic contact bodies with variation moduli E_{z1} and E_{z2} along the z -direction.

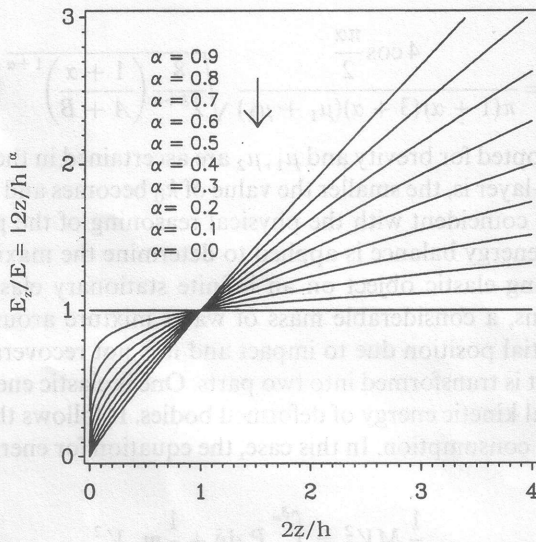


Fig. 2. Dimensionless elastic modulus varying with z and α .

written as

$$E_{z1} = E_1 \left| \frac{z}{h_1} \right|^\alpha = E_1 \left| \frac{2z}{h} \right|^\alpha \tag{1}$$

and

$$E_{z2} = E_2 \left| \frac{z}{h_2} \right|^\alpha = E_2 \left| \frac{2z}{h} \right|^\alpha \tag{2}$$

where $h_1 + h_2 = h$ and $h_1 = h_2 = h/2$ is assumed for the brevity of derivations.

Based on general results [14], a new expression for impact force is derived for the evaluation of film effects in the form

$$\delta_0 = \frac{f(\varepsilon)}{(m_\alpha)^{1+\alpha}} \left[\pi \kappa \frac{(1+\alpha)(3+\alpha)}{4 \cos \frac{\pi\alpha}{2}} \left(\frac{A+B}{1+\alpha} \right)^{(1+\alpha)/2} P_r \right]^{2/(3+\alpha)} \tag{3}$$

where

$$f\left(\frac{n_\alpha}{m_\alpha}\right) = \varepsilon^{-\alpha} \int_0^1 \left[1 - (1 - \varepsilon^2) \sin^2 \frac{\pi\phi}{2} \right]^{-(1+\alpha)/2} d\phi = f(\varepsilon). \tag{4}$$

Details for deriving Eqns (3) and (4) are given in the Appendix for compactness.

To be consistent with the conventional representation of Eqn (3) for $\alpha = 0$ [15], a geometric parameter $\lambda = f(\varepsilon)8^{1/(3+\alpha)}/(m_\alpha)^{1+\alpha}$ is introduced into Eqn (3) and then it is converted to

$$\delta_0 = \lambda \left[\frac{1}{\sqrt{8}} \frac{\pi \kappa (1+\alpha)(3+\alpha) \left(\frac{A+B}{1+\alpha}\right)^{(1+\alpha)/2}}{4 \cos \frac{\pi \alpha}{2}} \right]^{2/(3+\alpha)} P_r^{2/(3+\alpha)} \quad \text{or} \quad P_r = k_0 \delta_0^{(3+\alpha)/2} \quad (5)$$

where stiffness k_0 of the contact system is determined by

$$k_0 = k_0(\alpha) = \frac{4 \cos \frac{\pi \alpha}{2}}{\pi(1+\alpha)(3+\alpha)\kappa} \sqrt{\frac{8}{\lambda^{3+\alpha}} \left(\frac{1+\alpha}{A+B}\right)^{1+\alpha}} \quad (6)$$

Variations of λ with θ_α and α are listed in Table 1. When $\alpha = 0$ the values of λ are in agreement with results for homogeneous contact problems [15]. The effect of the layer thickness h on k_0 between two contact bodies can be found as

$$k_0 = \frac{4 \cos \frac{\pi \alpha}{2}}{\pi(1+\alpha)(3+\alpha)(\mu_1 + \mu_2)} \sqrt{\frac{8}{\lambda^{3+\alpha}} \left(\frac{1+\alpha}{A+B}\right)^{1+\alpha} \left(\frac{2}{h}\right)^\alpha} \quad (7)$$

Here $h_1 = h_2 = h/2$ is adopted for brevity and μ_1, μ_2 are ascertained in the Appendix. It follows from Eqn (7) that the thicker a layer is, the smaller the value of k_0 becomes and therefore P_r decreases with the increase of h . This is coincident with the physical reasoning of the problem.

Next, the principle of energy balance is applied to determine the maximum contact force for the normal strike of a moving elastic object on an infinite stationary elastic medium. According to experimental observations, a considerable mass of water mixture around a local contact zone is moved away from its initial position due to impact and it is not recoverable. Therefore, the kinetic energy of a moving object is transformed into two parts. One is elastic energy that is stored in bodies and the other part is local kinetic energy of deformed bodies. It follows that a reliable model should count this kind of energy consumption. In this case, the equation for energy balance is written in the form

$$\frac{1}{2} MV_0^2 = \int_0^{\delta_m} P_r d\delta + \frac{1}{2} m_x V_x^2 \quad (8)$$

Table 1. Material and geometric parameters for the Hertz contact of two inhomogeneous bodies

$\theta^\circ \backslash \lambda$	α									
	0.0	0.1	0.2	0.3	0.4	0.5	0.6	0.7	0.8	0.9
5	0.577	0.551	0.532	0.519	0.509	0.503	0.500	0.499	0.499	0.502
10	0.859	0.828	0.797	0.770	0.756	0.749	0.727	0.723	0.710	0.712
15	1.049	1.013	0.975	0.956	0.931	0.909	0.891	0.888	0.879	0.866
20	1.203	1.170	1.129	1.100	1.077	1.053	1.038	1.020	1.007	0.994
25	1.341	1.294	1.258	1.228	1.204	1.178	1.155	1.136	1.121	1.107
30	1.451	1.407	1.370	1.339	1.305	1.283	1.257	1.238	1.221	1.203
35	1.551	1.507	1.463	1.432	1.399	1.374	1.352	1.326	1.310	1.294
40	1.634	1.587	1.550	1.516	1.484	1.457	1.431	1.405	1.384	1.366
45	1.712	1.665	1.625	1.589	1.554	1.524	1.498	1.475	1.453	1.432
50	1.775	1.730	1.690	1.652	1.619	1.587	1.560	1.536	1.513	1.491
55	1.829	1.785	1.744	1.708	1.673	1.643	1.614	1.588	1.564	1.543
60	1.875	1.833	1.790	1.753	1.718	1.690	1.659	1.633	1.610	1.586
65	1.915	1.870	1.829	1.792	1.757	1.724	1.697	1.672	1.646	1.623
70	1.945	1.902	1.859	1.823	1.788	1.757	1.730	1.702	1.675	1.652
75	1.970	1.925	1.885	1.847	1.813	1.783	1.753	1.725	1.700	1.675
80	1.987	1.943	1.902	1.865	1.831	1.798	1.770	1.741	1.714	1.691
85	1.996	1.953	1.912	1.875	1.840	1.808	1.778	1.751	1.725	1.701
90	2.000	1.956	1.915	1.878	1.843	1.811	1.782	1.754	1.728	1.704

where m_x and V_x represent the effective mass and average velocity of the local zone, respectively. With no appearance of m_x or V_x , the meaning of Eqn (8) for homogeneous bodies is illustrated in [6]. After replacement of δ_0 by δ , substitution of Eqn (5) into Eqn (8) yields

$$\frac{1}{2} V_0^2 (M - M_x) = \frac{2k_0}{5 + \alpha} \delta_m^{(5+\alpha)/2} \quad (9)$$

where $M_x = m_x V_x^2 / V_0^2$ is also called effective mass. In terms of $P_m = k_0 \delta_m^{(\alpha+3)/2}$, the expression for the maximum impact force is given after calculations by

$$P_m = k_0^{2/(5+\alpha)} \left[\frac{5 + \alpha}{4} (M - M_x) V_0^2 \right]^{(3+\alpha)/(5+\alpha)} \quad (10)$$

In Eqn (10), M_x is an unknown parameter. It is very difficult to determine its exact form. However, major physical factors relating to M_x are clear. First, M_x vanishes when α or h is equal to zero and second, when V_0 is very large the inertia effect of a local zone is relatively small. In this case, it is reasonable to assume $M_x \propto \sqrt{\alpha h / V_0^2}$ and then one obtains $M_x = c \sqrt{\alpha h / V_0^2}$ where c and γ are physical constants which are determined by experiments. In order to have a convenient equation for the impact test of a freely falling ball, with no loss of physical meaning, M_x is rewritten as

$$M_x = c \sqrt{\frac{\alpha h}{H^\beta}} \quad (11)$$

where β is also a physical constant and H denotes the height of the falling ball. Substitution of Eqn (11) into Eqn (10) produces

$$P_m = k_0^{2/(5+\alpha)} \left[\frac{5 + \alpha}{2} \left(M - c \sqrt{\frac{\alpha h}{H^\beta}} \right) Hg \right]^{(3+\alpha)/(5+\alpha)} \quad (12)$$

where V_0^2 is replaced by $2Hg$. This is a basic equation for the analysis of impact contact with a water-mixture film.

3. EXPERIMENT

A series of impact tests have been implemented by the authors for verification of Eqn (12) through simulation of a water-mixture film. The measurement system consists of a four-component 9273-dynamometer, three dual mode amplifiers, an FFT spectrum analyzer and a PC-computer. To evaluate the potential influence of force components in x - and y -directions, their values vs time are measured simultaneously along with the normal impact force (z -direction) and plotted on a computer screen through the spectrum analyzer. For the impact test setup, the sample rate ranges in frequency from 200 to 500 kHz.

As shown in Fig. 3 a stainless steel plate of $15 \times 15 \times 1$ (cm) is fastened tightly by screws upon the dynamometer serving as an infinite target medium. A stainless steel ball is chosen as the striking object. Its mass is $M = 5.5 \times 10^{-3}$ and diameter $2R_1 = 2R'_1 = 11.112 \times 10^{-3}$. The moduli E_1 and E_2 of the plate and ball are both 20.4×10^{10} [16] and the Poisson ratios ν_1 and ν_2 are both 0.3. A plastic border of $10 \times 11 \times 2.5$ (cm) is adhered on the steel plate for containing water and its mixtures.

Before considering the film effects, Eqn (12) for $\alpha = 0$ is applied to calibrate the entire experimental setup. Substitution of known geometric and material data into Eqn (12) leads to

$$P_m = k_0^{2/5} \left(\frac{5}{4} M V_0^2 \right)^{3/5} = k_0^{3/5} \left[\frac{5}{2} M H g \right]^{3/5} = 3.14 \times 10^3 H^{3/5} \quad (13)$$

A comparison between the theoretical prediction and experimental data is plotted in Fig. 4(a) and shows very good agreement. Throughout this paper, every experimental datum is the average value of three repetitive tests. A typical test pattern for P_m vs time is given in Fig. 4(b) where the bold curve denotes the voltage which is directly proportional to the impact force in the z -direction, i.e. P_m and the two light curves denote those in the x - and y -directions. Digital records show that when the force in the z -direction reaches a peak value, the forces in the x - and y -directions are very small. It is important to point out that deviation between theoretical and experimental analyses becomes

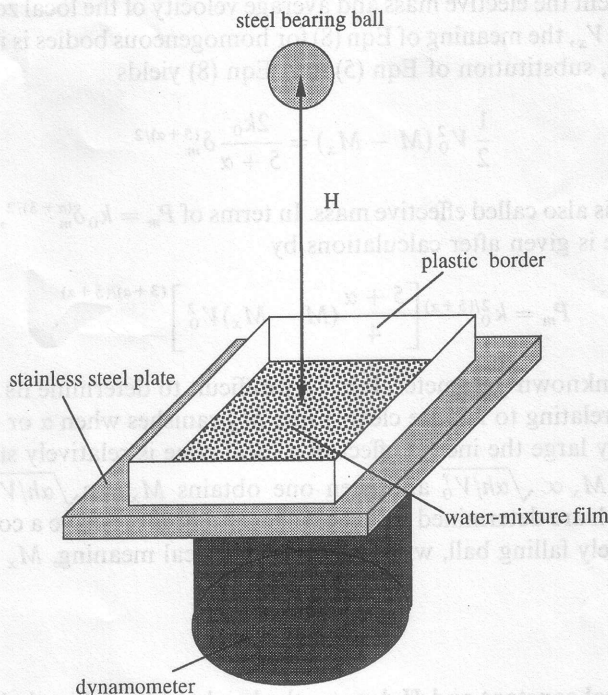


Fig. 3. The pattern of experimental setup for impact tests.

significant when $H > 0.3(\text{m})$ or $V_0 > 2.42(\text{m/s})$. It implies that non-negligible plastic deformation may occur if impact velocity is large. Some reviews about the permanent deformation are given in the work [17]. For brittle target materials, such as ceramics, the accuracy of Eqn (13) could be improved because of small plastic deformation before damage. Further experimental results for film effects demonstrate that different types of water-mixture films exhibit similar physical behavior. Two of them are described in detail below.

It is seen in Fig. 4(b) that the measurement curves for impact force exhibit an oscillating appearance. According to the experimental setup, this phenomenon results from the vibration of the plate between the dynamometer and the ball. Because a high frequency band is assigned during the measurement, all the recordable signals can appear on the patterns once the ball makes contact with the plate. Similar phenomena also can be found in other impact tests (e.g. Ref. [12], p. 162, Fig. 2) using different measuring systems. A single impulse signal can be plotted so long as the time interval is limited within a small domain, however, the entire response of the measurement system is incomplete when such a treatment is chosen. Strictly speaking, P_m should be determined by using the formula $P_m = K_m V_m$ where V_m is the maximum voltage of the dynamometer output, K_m is the coefficient of a magnifier. Because of the existence of potential disturbances from the measuring system, a modification constant c_f is introduced to eliminate the errors in the form

$$c_f = V_m K_m / P_m^t \quad (14)$$

where P_m^t is a theoretical maximum value of the impact force. All the subsequent experimental maximum values of the impact force are calculated by $P_m^e = K_m V_m / c_f$.

The first type of water-mixture film is made of steel powder and water. Steel powder is produced by wearing a U-type steel plate on a grinding machine. After powder and water in the pool shown in Fig. 3 are well stirred, extra water above the powder is drawn out from the pool. In order to measure the thickness of the water-mixture film, a sheet of aluminum film is mounted on the steel target and in the meantime the water-mixture surface is smoothed to have the same height as the aluminum film. In this assignment, thickness h of the water-mixture film is about $3.565 \times 10^{-4}(\text{m})$. One should bear in mind that it is hard to obtain an accurate value for h since it is relevant to several factors, such as the volume ratio of powder to water and the asperity of the mixture surface. However, once a water-mixture film is made, one can find a very good match between theory and experiment.

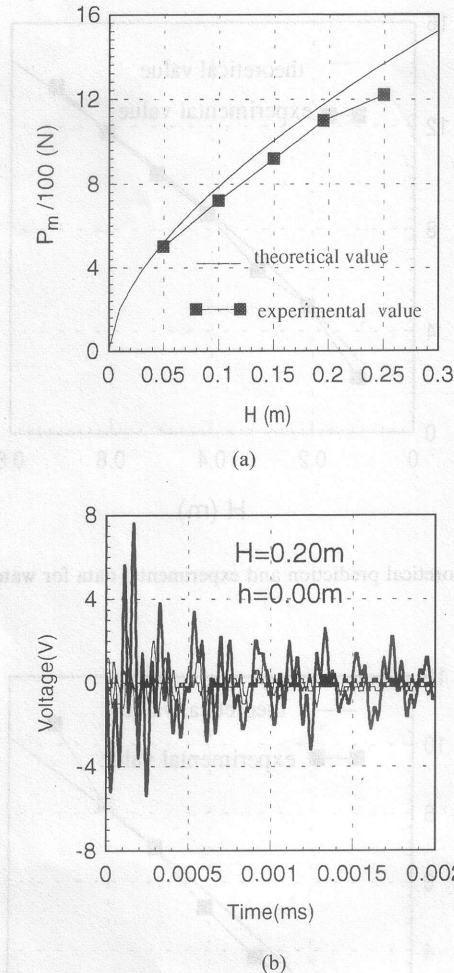


Fig. 4. Calibration of the measurement system: (a) a comparison between theory and experiment; (b) an example of experimental record.

Insertion of known parameters into Eqn (12) leads to

$$P_{mF} = k_0^{2/(5+\alpha)} \left[\frac{5+\alpha}{2} \times 10^{-2} \times \left(0.55 - 1.888c \sqrt{\frac{\alpha}{H^\beta}} \right) Hg \right]^{(3+\alpha)/(5+\alpha)} \quad (15)$$

In Eqn (15), α is limited by $0 < \alpha < 0.1$ for the current model according to the foregoing discussions as shown in Fig. 2. The key point now is to determine two unknown physical constants β and c . When $H = 0.20$, measurements give $P_m = 4.71 \times 10^2$. Calculations show that $\alpha = 0.08$, $c = 0.96$ and $\beta = 0.22$ are well-fitted with the experimental value of P_m . Consistently, data of subsequent tests are also in agreement with the prediction of Eqn (15), as illustrated in Fig. 5. One might note that a certain error appears in Fig. 5 in the vicinity of $H = 0$ but it is just a trivial case since impact velocity for $H \approx 0$ is very small.

The second type of water-mixture film is composed of water and garnet abrasives of mesh 80. Measurements give $h = 3.565 \times 10^{-4}$ (m), $\alpha = 0.07$, $c = 1.25$ and $\beta = 0.16$. As above, the theory for this case is consistent with the experiment as shown in Fig. 6. Note that the exponent α of water-steelpowder film is greater than that of the water-abrasive film, which suggests that the first one is harder than the second one. In comparison with steelpowder used here, abrasives in water are very loose granules. Thus, their viscosity is lower and they can be more easily moved away when they are subjected to impact. Consequently, the local kinetic energy $m_x V_x^2/2$ or M_x for the water-abrasive mixture becomes larger. In terms of Eqn (10), this is the main reason why an impact force associated with water-steelpowder film is greater than an impact force with water-abrasive film.

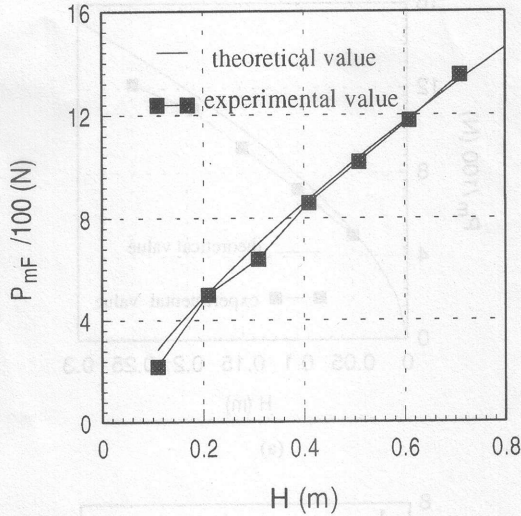


Fig. 5. The curves of theoretical prediction and experimental data for water-steelpowder film.

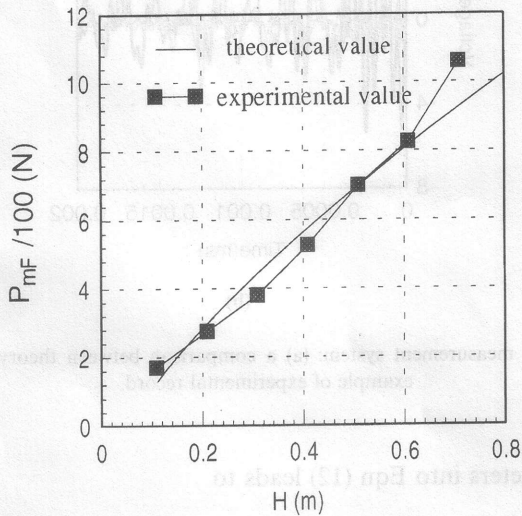


Fig. 6. The curves of theoretical prediction and experimental data for water-abrasive film.

In further analysis of water-mixture film effects, the ratio of the impact force P_m for dry contact to the impact force P_{mF} for film contact is introduced in the form

$$r_p = \frac{P_m}{P_{mF}} = \frac{k_0^{2/5}(0) \left[\frac{5}{2} MHg \right]^{3/5}}{k_0^{2/(5+\alpha)}(\alpha) \left[\frac{5+\alpha}{2} \left(M - c \sqrt{\frac{\alpha h}{H^b}} \right) Hg \right]^{(3+\alpha)/(5+\alpha)}} \quad (16)$$

Obviously, the larger r_p is, the greater the film effects become. For the two types of water-mixture films discussed above, r_p vs H is plotted in Fig. 7 where the potential plastic deformation of the local zone for dry contact, if any, is not considered. Therefore these results are more likely to be suitable for brittle materials. It can be seen that effects of water-mixture film varies greatly with the level of kinetic or impact energy. Compared with dry contact, impact force can be tremendously reduced by film, provided that impact energy is limited within the range of small values, for example, $H < 0.25 \sim 0.30$ (m) or $V_0 < 2.21 \sim 2.43$. Once impact energy increases up to a certain limitation, however, film effects on impact force rapidly reach a stable value and become less noticeable. Most

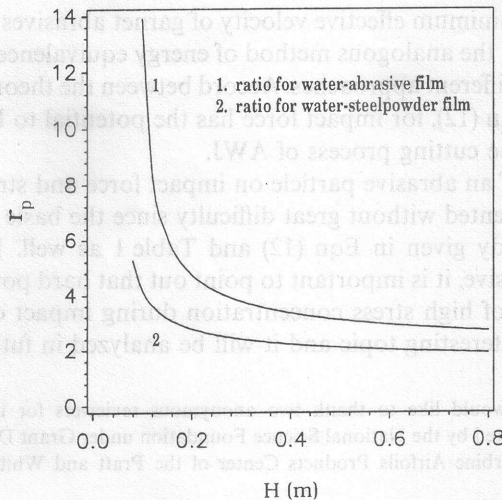


Fig. 7. Ratio r_p of the impact force for dry contact to the impact force for water-mixture film contact.

importantly, the height H corresponding to the initial stable stage of r_p appears to be a physical invariant. This finding provides a new analogy method to estimate the minimum effective velocity that an abrasive in waterjet must have; let kinetic energy of an abrasive equate that of a falling ball, and the expression for the velocity V_p of the abrasive with mass M_p is obtained

$$V_p = \sqrt{\frac{M}{M_p}} V_0 = \sqrt{2Hg \frac{M}{M_p}}. \quad (17)$$

According to known data for garnet abrasives of mesh 60 [18–19], calculations lead to

$$M_p = \frac{\pi}{6} (4.6 \times 10^{-4})^3 \times \left(\frac{3.4 + 4.3}{2} \right) \times 10^3 = 1.962 \times 10^{-7} \quad (18)$$

and then

$$V_p = \sqrt{2 \times 9.8 \times \frac{5.5 \times 10^{-3}}{1.962 \times 10^{-7}} H} = 741.2 \sqrt{H}. \quad (19)$$

In addition, the data given in Fig. 7 indicate that ratio r_p begins to get into the stable state when $H = 0.25 \sim 0.30$. Therefore, the minimum velocity V_p of abrasives for an effective cutting process of AWJ is about 370–406. The prediction for V_p in [18] is over 300 and two specific values given in [19] are 305 and 396, making use of a momentum balance approach. It follows that results derived from two different methods agree with each other.

From the contact mechanics point of view, these results provide a clear pattern for understanding sensitive variations of acoustic emission signals of AWJ with different flow-out conditions. For partial cutting, the velocity of some abrasives may be decreased by relatively slow flow before striking a target. As a result, they may no longer carry sufficient impact energy to either penetrate a water-mixture film or cut the target surface. This could be the reason why the partial-penetration operation has weaker acoustic emission signals than the full-penetration operation does. In addition, the results reported here are also applied to establish a general erosion model for predicting the drilling and cutting depth by AWJ [20–22].

4. CONCLUSION AND DISCUSSION

Effects of a water-mixture film on impact force are well-modeled by the inhomogeneously-layered contact theory. In comparison with dry contact, the maximum impact force is significantly reduced by a water-mixture film when impact energy of an object is low; when impact energy increases up to a certain critical value the effects reach a stable state and become less influential. This finding appears to be similar to that reported in [8] for one-phase squeeze film, which used the fluid

mechanics approach. The minimum effective velocity of garnet abrasives with the size of mesh 60 is estimated for AWJ by using the analogous method of energy equivalence and its value is consistent with previous results from different approaches. Accord between the theory and experiment suggests that the new expression, Eqn (12), for impact force has the potential to be an essential equation in quantitatively simulating the cutting process of AWJ.

The effect of sharpness of an abrasive particle on impact force and stress is not discussed in this paper but it can be implemented without great difficulty since the basic equations and parameters for this influence are already given in Eqn (12) and Table 1 as well. Moreover, apart from the sharpness of a striking abrasive, it is important to point out that hard powder particles of a mixture can also act as the source of high stress concentration during impact contact somewhat like the rough surface. This is an interesting topic and it will be analyzed in future work.

Acknowledgement—The authors would like to thank two anonymous reviewers for their constructive and insightful comments. This research is supported by the National Science Foundation under Grant DMI-9523010 and partially by the Allison Engine Company, the Turbine Airfoils Products Center of the Pratt and Whitney and the Flow International Corporation.

APPENDIX A

From the general results of [14], the relevant parameters are listed below

$$\frac{b}{a} = \frac{n_x}{m_x} = \varepsilon, \quad (\text{A1})$$

$$\cos \theta_x = \frac{|B - A|}{B + A}, \quad (\text{A2})$$

$$\sigma_u = \frac{3 + \alpha}{2} \frac{P_r}{\pi ab}, \quad (\text{A3})$$

$$\pi(1 + \alpha)\kappa\sigma_u \int_0^{\frac{\pi}{2}} c^{1-\alpha}(\phi) d\phi = \delta_0 \cos \frac{\pi\alpha}{2}, \quad (\text{A4})$$

$$a = m_x \left[\frac{\pi(1 + \alpha)^2(3 + \alpha)}{4} \frac{\kappa P_m}{\cos \frac{\pi\alpha}{2}} \frac{1}{A + B} \right]^{1/(3 + \alpha)} \quad (\text{A5})$$

where values of m_x and n_x are tabulated in [14] and

$$c(\phi) = b[1 - (1 - \varepsilon^2) \sin^2 \phi]^{-1/2}, \quad (\text{A6})$$

$$\kappa = \kappa_1 + \kappa_2, \quad (\text{A7})$$

$$\kappa_i = \frac{(1 - \nu_i) D_i q_i \sin \frac{\pi q_i}{2} \Gamma\left(\frac{1 + \alpha}{2}\right)}{4G_i(1 + \alpha) \sqrt{\pi} \Gamma\left(1 + \frac{\alpha}{2}\right)} h_i^2 = \mu_i h_i^2, \quad (i = 1, 2) \quad (\text{A8})$$

$$G_i = \frac{E_i}{2(1 + \nu_i)}, \quad (\text{A9})$$

$$D_i = \frac{2^{1 + \alpha} \Gamma\left(1 + \frac{1 + \alpha + q_i}{2}\right) \Gamma\left(1 + \frac{1 + \alpha - q_i}{2}\right)}{\pi \Gamma(2 + \alpha)}, \quad (\text{A10})$$

$$q_i = \left[(1 + \alpha) \left(1 - \frac{\alpha \nu_i}{1 - \nu_i} \right) \right]^{1/2}, \quad (\text{A11})$$

$$B - A = \pm \frac{1}{2} \left[\left(\frac{1}{R_1} - \frac{1}{R_1'} \right)^2 + \left(\frac{1}{R_2} - \frac{1}{R_2'} \right)^2 + 2 \left(\frac{1}{R_2} - \frac{1}{R_1'} \right) \left(\frac{1}{R_2} - \frac{1}{R_2'} \right) \cos \Phi \right]^{1/2}, \quad (\text{A12})$$

$$A + B = \frac{1}{2} \left(\frac{1}{R_1} + \frac{1}{R_1'} + \frac{1}{R_2} + \frac{1}{R_2'} \right). \quad (\text{A13})$$

More details about geometric meanings of Eqns (A12, A13) are given in [23]. From Eqns (A3, A4), one obtains

$$\pi \kappa \frac{(1 + \alpha)(3 + \alpha)}{4} \frac{P_r}{a^{1 + \alpha}} f\left(\frac{n_x}{m_x}\right) = \delta_0 \cos \frac{\pi\alpha}{2} \quad (\text{A14})$$

where

$$f\left(\frac{n_x}{m_x}\right) = \varepsilon^{-\alpha} \int_0^1 \left[1 - (1 - \varepsilon^2) \sin^2 \frac{\pi\phi}{2} \right]^{-((1-\alpha)/2)} d\phi = f(\varepsilon). \quad (\text{A15})$$

After substitution of Eqn (A5) into Eqn (A14), tedious derivations lead to

$$\delta_0 = \frac{f(\varepsilon)}{(m_x)^{1+\alpha}} \left[\pi\kappa \frac{(1+\alpha)(3+\alpha)}{4 \cos^2 \frac{\pi\alpha}{2}} \left(\frac{A+B}{1+\alpha} \right)^{(1+\alpha)/2} P_r \right]^{2/(3+\alpha)} \quad (\text{A16})$$

$$k_0 = \frac{4 \cos^2 \frac{\pi\alpha}{2}}{\pi(1+\alpha)(3+\alpha)(\mu_1 + \mu_2)} \sqrt{\frac{8}{\lambda^{3+\alpha}} \left(\frac{1+\alpha}{A+B} \right)^{1+\alpha}} \left(\frac{2}{h} \right)^\alpha \quad (\text{A17})$$

REFERENCES

1. Shipway, P. H. and Hutchings, I. M., Fracture of brittle sphere under compression and impact loading: I. Elastic stress distributions. *Philosophical Magazine A*, 1993, **67**, 1389–1404.
2. Shipway, P. H. and Hutchings, I. M., Fracture of brittle sphere under compression and impact loading: II. Results for lead-glass and sapphire spheres. *Philosophical Magazine A*, 1993, **67**, 1405–1421.
3. Campbell, C. S., Impulse strength in rapid granular shear flows. *Acta Mechanica*, 1994, **104**, 65–90.
4. Momber, A., Kwak, H. and Kovacevic, R., Investigations in abrasive waterjet erosion based on particle wear analysis. *ASME Journal of Tribology*, in press.
5. Mohan, R., Momber, A. and Kovacevic, R., On-line monitoring of depth of AWJ penetration using acoustic emission technique. *Jet Cutting Technology*, ed. A. Lichtarowicz, Kluwer, 1994, 649–663.
6. Yong, Z., Hanson, M. T. and Kovacevic, R., Topological measure of brittle fragmentation. *International Journal of Solids and Structures*, 1994, **31**, 391–415.
7. Yong, Z. and Hanson, M. T., A rational source of plane fractal and application to fragmentation analysis of thin plates. *Chaos, Solitons and Fractals*, 1996, **7**, 31–40.
8. Clark, H. M. and Burmeister, L. C., The influence of the squeeze film on particle impact velocities in erosion. *International Journal of Impact Engineering*, 1992, **3**, 415–426.
9. Sheldon, G. L. and Finnie, I., On the ductile behavior of nominally brittle materials during erosive cutting. *ASME Journal of Engineering for Industry*, 1966, **105**, 215–222.
10. Knight, C. G., Swain, M. V. and Chaudhri, M. M., Impact of small steel on glass surfaces. *Journal of Material Science*, 1977, **12**, 1573–1586.
11. Benchaita, M. T., Griffith, P. and Rabinowicz, E., Erosion of metallic plate by solid particles entrained in a liquid jet. *ASME Journal of Engineering for Industry*, 1983, **105**, 215–222.
12. Lundberg, J., Lubrication of machine elements during combined squeeze and sliding motion. *Wear*, 1993, **169**, 161–166.
13. Larsson, R. and Lundberg, J., Study of lubricated impact using optical interferometry. *Wear*, 1995, **190**, 184–189.
14. Yong, Z. and Hanson, M. T., Three-dimensional crack and contact problems with a general geometric configuration. *Journal of Mechanics and Physics of Solids*, 1994, **42**, 215–239.
15. Timoshenko, S. and Goodier, J. N., *Theory of Elasticity*. McGraw-Hill, New York, 1951.
16. Johnson, W., *Impact Strength of Materials*. Edward Arnold, London, 1972.
17. Goldsmith, W., *Impact*. Edward Arnold Ltd, London, 1960.
18. Hashish, M., Optimization factors in abrasive-waterjet machine. *ASME Journal of Engineering Material and Technology*, 1991, **113**, 29–37.
19. Hashish, M., A modeling study of metal cutting with abrasive-waterjets. *ASME Journal of Engineering Material and Technology*, 1984, **106**, 88–100.
20. Yong, Z. and Kovacevic, R., Fundamentals of constructing particle-laden jetflow by fractal point sets and predicting 3D solid erosion rates. *Chaos, Solitons and Fractals*, in press.
21. Kovacevic, R. and Yong, Z., Modeling of 3D abrasive waterjet machining—part I: theoretical basis. *Jet Cutting Technology*, in press.
22. Yong, Z. and Kovacevic, R., Modeling of 3D abrasive waterjet machining—part II: simulation of machining. *Jet Cutting Technology*, in press.
23. Johnson, K. L., *Contact Mechanics*. Cambridge University Press, Cambridge, 1985.